ACS APPLIED MATERIALS & INTERFACES

Research Article

www.acsami.org

Electro-oxidation of Ascorbic Acid by Cobalt Core–Shell Nanoparticles on a H-Terminated Si(100) and by Nanostructured Cobalt-Coated Si Nanowire Electrodes

Liyan Zhao, Kristine Liao, Mark Pynenburg, Louis Wong, Nina Heinig, Joseph P. Thomas, and K. T. Leung*

WATLab, and Department of Chemistry, University of Waterloo, Waterloo, Ontario, Canada N2L 3G1

Supporting Information

ABSTRACT: Determination of the concentration of ascorbic acid in a solution has attracted intense recent interest. Here we demonstrate the feasibility of electro-oxidation of ascorbic acid on spherical cobalt core–shell nanoparticles (10-50 nm dia.) prepared by electrochemical deposition on a H-terminated Si(100) substrate. Depth-profiling X-ray photoelectron spectroscopy reveals that these nanoparticles consist of a metallic cobalt core covered by a $Co(OH)_2$ shell without any evidence of CoO_x. Glancing-incidence X-ray diffraction studies further show that the metallic Co core consists of a mixture of hexagonal close packed and face centered cubic structures, the relative composition of which can be easily controlled by the deposition potential. We further demonstrate that when these Co nanoparticles are deposited on a high-surface-area electrode as provided by a Si nanowire template, the resulting nanostructured Co-coated Si nanowire electrode offers a promising high-performance sensor platform for ascorbic acid detection.

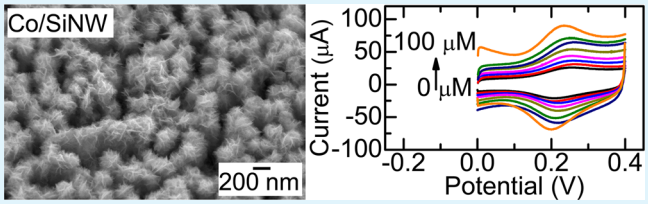

KEYWORDS: *cobalt core–shell nanoparticles, electrodeposition, silicon nanowire electrode, SEM, XPS, GIXRD, electro-oxidation of ascorbic acid*

1. INTRODUCTION

Ascorbic acid is a powerful antioxidant naturally present in many fruits and vegetables, and it is indispensable for building an immune system against many diseases.[1] Because of its biological and technological importance, there is a continued interest to develop rapid and sensitive methods for routine determination of its concentration in the food industry. Many techniques have been used for the quantitative determination of ascorbic acid, and they include titration,[2] liquid chromatography,[3] ultraviolet spectroscopy,[4] fluorimetry,[5] flow injection analysis,[6] turbidimetry,[7] and electrochemical methods. Among them, electrochemistry offers a fast and reliable analysis technique, often employing various high surface area electrodes, including modified carbon-paste,[8] modified carbon ceramic,[9] modified pyrolytic graphite,[10−12] 3D nanoporous gold thin film,[13] Ni–Pt alloy,[14] Cu(II) zeolite-modified Pt,[15] B-doped diamond,[16] and modified glassy carbon electrodes (GCE).[17,18] It has been reported that GCE modified by Co-doped hematite nanoparticles exhibits not only a higher anodic current response with a shift in positive potential than the bare GCE but also enhanced electrochemical sensing performance for ascorbic acid than GCE modified by undoped hematite nanoparticles.[19] Tian et al. have prepared GCE modified by an electroplated (thick) Co film and demonstrated their superior electrocatalytic activity to the oxidation of ascorbic acid. They also reported the best biosensor to date, with a fast response time of less than 3 s, an excellent linear relationship in the concentration range of 3×10^{-7} to 1×10^{-4} M, and a detection limit of 2×10^{-7} M.[20] These studies therefore suggest that Co nanostructures could offer potentially excellent catalytic performance enhancement for the electro-oxidation of ascorbic acid.

Silicon is a good biosensor substrate because of its high reliability and low output impedance.[21] In addition to integrated sensor application, the study of metallic nanostructures deposited on Si substrates is also important to microelectronic, optoelectronic and magnetic storage. In particular, Co nanostructures deposited on a Si substrate has attracted a lot of attention due to its magnetic behavior and catalytic properties. Several techniques to prepare Co nanostructures on a Si support have been reported. Kwon et al. have reported thermal atomic layer deposition of ca. 1 monolayer Co on a H-terminated Si substrate using the cobalt carbonyl complex (tertbutylallylcobalttricarbonyl).[22] Pető et al. prepared nanosized Co particles by Ar ion sputtering of a 4–5 nm thick, "islandlike" Co film predeposited on a Si(111) substrate by electron beam evaporation.[23,24] The resulting Co nanoparticles (NPs) exhibit a "raftlike" morphology with a lateral dimension of 5-10 nm and a height of 2 nm. Koch et al. prepared Co nanoclusters of ∼8 nm diameter on a p-Si(100)

Received: October 1, 2012
Accepted: March 14, 2013
Published: March 14, 2013

   dx.doi.org/10.1021/am3021763 | ACS Appl. Mater. Interfaces 2013, 5, 2410–2416

substrate by using a cluster deposition source, in which a supersaturated metal vapour beam was generated by sputtering a Co target in an Ar atmosphere.[25] Co nanoclusters were then obtained by gas aggregation in the condensation chamber. Another technique involved the use of a colloidal solution of Co NPs covered by surfactants in a wet-chemistry method. Kalska et al. prepared thin films of Co NPs of 8, 10, and 12 nm dia. on a Si wafer by drying droplets of the colloidal NP solution.[26] Colloidal Co NPs of 10−12 nm dia. have also been deposited on a Si(100) substrate by spin-coating with[27] and without the presence of a magnetic field.[28] As a simple, low-cost, high-throughput synthesis technique, electrodeposition offers a potential way of preparing Co nanostructures on a Si substrate from a precursor solution containing Co ions. To date, however, not much work has been reported on metallic Co nanostructure growth on Si substrates by electrodeposition. Recently, Curry et al. electrodeposited perpendicular metallic Co nanowires (with an average diameter of 20 nm) on a H-terminated Si(111) substrate using the coblock polymer templating method.[29] Moina et al. reported the preparation of nano-sized Co nuclei on p-Si(111) by electrodeposition at −0.7 V (with respect to a saturated calomel electrode), for which "flat spheroids", with maximum heights of ∼65 nm, were uniformly distributed on the Si surface.[30] Here, we use electrodeposition to prepare Co NPs on a H-terminated Si(100) substrate, with good control of their morphology and their resulting properties. These Co NPs are found to consist of a metallic Co core and a $Co(OH)_2$ shell. We demonstrate that these as-electrodeposited Co NPs can be used as catalysts for electro-oxidation of ascorbic acid in an alkaline solution, and we characterize their performance by cyclic voltammetry. To increase their efficacy, we employ a high-surface-area Si nanowire (SiNW) substrate for the growth of these nanostructured cobalt electrodeposits and show that they can be used as a high-performance sensor platform for analysis of the concentration of ascorbic acid.

2. EXPERIMENTAL DETAILS

Electrodeposition of metallic Co on H−Si(100) was performed in a three-electrode cell with a potentio/galvanostat electrochemical workstation (CH Instruments 660A). The working electrode was a p-type, single-side-polished, rectangular Si(100) chip (15 × 2.5 mm^2, 0.4 mm thick, with a resistivity of 1.0-1.5 mΩ cm), which has been H-terminated by a standard procedure.[31] The Si chip was cleaned by using the RCA method, etched in an aqueous HF (2%) solution to remove the native oxide layer, and thoroughly rinsed with filtered de-ionized water (with resistivity of 18.2 MΩ cm). A standard Ag/AgCl reference electrode and a platinum-wire counter electrode were used in all the electrodeposition experiments. In a deoxygenated aqueous solution of 0.005 M $CoSO_4$, mixed with 0.2 M KCl and 0.2 M H_3BO_3 as the supporting electrolyte, Co nanostructures were deposited on the H−Si(100) substrate by amperometry at a constant potential. It should be noted that all the potentials reported in this work were relative to the Ag/AgCl reference electrode unless stated otherwise. After the deposition, the sample was thoroughly rinsed with de-ionized water and dried in N_2, before further analysis of the resulting electrodeposits. The electro-oxidation of ascorbic acid was also studied in the same electrochemical workstation, with the as-electrodeposited Co NPs on the Si substrate used as the working electrode. In a deoxygenated aqueous solution of 0.1 M NaOH and various concentrations of L-ascorbic acid (0, 2.5, 5, 10, and 20 mM), cyclic voltammetric scans were performed between −0.4 V and 0.8 V at a scan rate of 10 mV s^{-1}.

We also prepared a Si nanowire (NW) substrate for Co nanostructured electrodeposit using a standard method.[32] The H−Si(100) chip was immersed in 5 M HF and 0.02 M $AgNO_3$ for 10 min and subsequently rinsed with de-ionized water. In order to remove the metallic Ag deposit, we used a solution of concentrated HNO_3 in H_2O (1:1 in volume) to wash the resulting SiNW substrate. The Ag-free SiNW substrate (the absence of Ag confirmed by XPS, not shown) was then thoroughly rinsed with de-ionized water and dried by N_2, for subsequent use as a working electrode for the electrodeposition of nanostructured Co at −1.4 V for 10 min in a solution of 0.005 M $CoSO_4$, 0.2 M KCl and 0.2 M H_3BO_3. The nanostructured Co film deposited on the SiNW substrate was then used as the working electrode for cyclic voltammetric scans between 0 V and 0.4 V at a scan rate of 10 mV s^{-1} in a deoxygenated aqueous solution of 0.1 M NaOH and various concentrations of L-ascorbic acid (0, 0.1, 0.5, 1, 5, 10, 50, and 100 μM).

The surface morphology of the Co electrodeposits was characterized by scanning electron microscopy (SEM) in a LEO 1530 field-emission microscope, while the corresponding chemical composition was analyzed by X-ray photoelectron spectroscopy (XPS) as a function of Ar ion sputtering time. The depth-profiling XPS experiment was conducted in a Thermo-VG Scientific ESCALab 250 Microprobe equipped with a monochromatic Al Kα X-ray source (1486.6 eV), at a typical energy resolution of 0.4-0.5 eV full-width at half-maximum. Argon sputtering was performed over a rastered area of 3×3 mm^2 of the sample at an ion beam energy of 3 keV and sample current density of 110 nA mm^{-2}. The crystallographic nature of the electrodeposits was determined by glancing-incidence X-ray diffraction (GIXRD) at an incidence angle of 0.6°, with the Cu Kα anode operating at 45 kV and 35 mA.

3. RESULTS AND DISCUSSION

In the electrodeposition experiments, the common parameters used to control the morphology of the nanodeposits are electrolyte concentration, deposition potential and deposition time. For the solution containing a low $CoSO_4$ concentration of 0.005 M, along with 0.2 M KCl and 0.2 M H_3BO_3 (with a pH of 4.34), an electrodeposition potential of −1.4 V is chosen. Because of the acidic electrolytes, hydrogen evolution is observed simultaneously during the cobalt deposition. The addition of H_3BO_3 provides a buffer to prevent local pH rise caused by the concurrent hydrogen evolution reaction, therefore reducing the electrodeposition of hydroxide species through the reaction: $Co^{2+} + 2H_2O + 2e^- \rightarrow H_2 + Co(OH)_2$.[33] Only near-spherical Co NPs with an average diameter of 6 nm are obtained on the H−Si(100) substrate at a very short deposition time of 1 ms (Figure 1a). With the deposition time

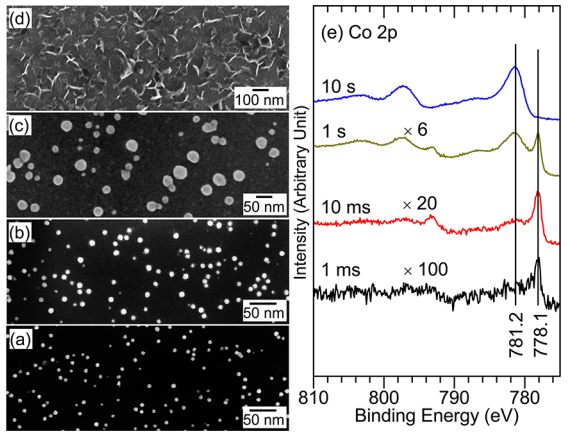

Figure 1. SEM images of Co electrodeposits obtained in a solution of 0.005 M $CoSO_4$, 0.2 M KCl, and 0.2 M H_3BO_3 at −1.4 V (vs Ag/AgCl) for (a) 1 ms, (b) 10 ms, (c) 1 s, and (d) 10 s, and (e) their corresponding XPS spectra of the Co 2p region.

dx.doi.org/10.1021/am3021763 | ACS Appl. Mater. Interfaces 2013, 5, 2410−2416

increased to 10 ms, the average NP size is found to increase to 17 nm dia. (Figure 1b). For 1 s deposition time, the Co NPs exhibit a wide size distribution of 10-50 nm (Figure 1c). A continuous, uniform Co film with ridge-like structures appears at a longer deposition time of 10 s (Figure 1d).

We have also investigated the pH effect on the Co NP deposition. In particular, by increasing the concentration of H_3BO_3 from 0.2 M to 0.8 M, the solution becomes more acidic, with the corresponding pH changing from 4.34 to 3.50. The decrease in the pH evidently stops the deposition of Co NPs, which could be due to reactions of the electrodeposited metallic Co NPs with the acid. On the other hand, significantly more Co deposition is observed by using the solution with the same $CoSO_4$ concentration of 0.005 M and 0.2 M KCl but without H_3BO_3 (with a pH of 4.83), which indicates a dramatically higher deposition rate.

We show the corresponding Co 2p XPS spectra of the samples obtained with different deposition times in Figure 1e. For the 1 ms deposition, the spectrum appears weak due to the small amount of the deposits. The main Co $2p_{3/2}$ peak at 778.1 eV can be attributed to metallic Co, with no binding energy shift from the corresponding metallic bulk Co feature,[34] which indicates that the obtained Co NPs (of 6 nm dia. in size) are too big to exhibit any quantum size effect. It should be noted that oxidation of metallic Co is unavoidable for electrodeposition in an aqueous solution. Using a higher pass energy (40 eV), we could observe a weak but discernible Co $2p_{3/2}$ feature at 781.2 eV attributable to a thin $Co(OH)_2$ shell,[35] in addition to the main metallic Co feature at 778.1 eV (see the Supporting Information, Figure S1). For NPs obtained with electrodeposition for 10 ms and 1 s, their XPS spectra also show the presence of the broad $Co(OH)_2$ feature at 781.2 eV and the sharp metallic Co feature at 778.1 eV, with the intensity of the $Co(OH)_2$ feature relative to the metallic Co feature found to be larger for the 1s-deposition than that for the 10 ms deposition. For the Co nanostructured film obtained with the 10-s deposition, only the $Co(OH)_2$ feature at 781.2 eV is observed, indicating the presence of a rather thick $Co(OH)_2$ component larger than the escape depth of the photoelectrons (typically 2−10 nm).[36]

Figure 2 shows XPS spectra of Co 2p region as a function of total sputtering time for Co NPs obtained by 1 s electrodeposition at −1.4 V) in a 0.005 M $CoSO_4$ solution (mixed with 0.2 M KCl and 0.2 M H_3BO_3). Before sputtering, the sharp Co $2p_{3/2}$ ($2p_{1/2}$) feature at 778.1 eV (793.2 eV) and the broader Co $2p_{3/2}$ ($2p_{1/2}$) feature at 781.2 eV (797.1 eV) can be attributed to metallic Co and $Co(OH)_2$, respectively.[34,35] The weak broad Co $2p_{3/2}$ ($2p_{1/2}$) feature found at a higher binding energy of 786.9 eV (803.4 eV) has been assigned to a shakeup transition in $Co(OH)_2$ by Kim et al.,[35] which further confirms the presence of $Co(OH)_2$. Sputtering appears to reduce the intensities of the $Co(OH)_2$ features and increase that of the metallic Co feature. After 125 s of sputtering, the $Co(OH)_2$ features (representing the shell region of the NPs) have been completely removed while the metallic Co feature (representing the core region) reaches the maximum intensity, with a shoulder emerging at 778.7 eV. The latter feature can be assigned to cobalt disilicide, $CoSi_2$.[37] Further sputtering above 245 s begins to reduce the metallic Co features. The present depth-profiling XPS data therefore support that the Co NPs are composed of a metallic Co core with a sizeable $Co(OH)_2$ shell amounting to approximately 25% of the NP composition, as estimated from the fraction of the Co $2p_{3/2}$ intensity for

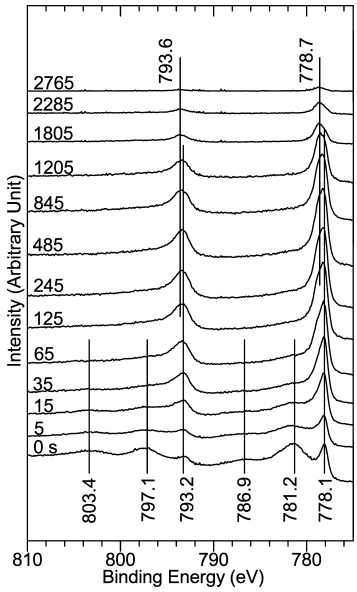

Figure 2. XPS spectra of Co 2p region for Co nanoparticles as-electrodeposited for 1 s in a solution of 0.005 M $CoSO_4$, 0.2 M KCl, and 0.2 M H_3BO_3 at −1.4 V (vs Ag/AgCl) as a function of Ar sputtering time.

$Co(OH)_2$ to the maximum total Co $2p_{3/2}$ intensity (for $Co(OH)_2$ plus metallic Co features) during sputtering.

Our depth-profiling XPS results therefore shows that the observed shell appears to remarkably contain only $Co(OH)_2$, without any form of Co oxides. In the study by Kim et al.,[35] the Co $2p_{3/2}$ features for the reference compounds of CoO and Co_3O_4 are reported at 780.3 eV and 779.9 eV, respectively. The absence of these higher binding energy features in our NPs therefore rules out the presence of CoO or Co_3O_4 inside the shell. Furthermore, post-annealing of as-deposited sample at 400 °C in a N_2 atmosphere shows a Co $2p_{3/2}$ feature at 779.9 eV, which confirms the formation of Co_3O_4. Upon sputtering this post-annealed sample, we also observe a Co $2p_{3/2}$ feature at 780.3 eV, attributable to CoO. These XPS depth-profiling spectra (see the Supporting Information, Figure S2) therefore verify that post-annealing could convert the $Co(OH)_2$ shell to a Co_3O_4 overlayer on a CoO shell. Because we conduct the electrodeposition in a deoxygenated aqueous solution, the metallic Co electrodeposits could easily react with water and form the $Co(OH)_2$ shell on the surface. Similar hydroxide formation is also observed for Ni,[38] but not for Fe[39] or Cu,[40] where only the oxide formation is found. The observed difference is possibly due to the reaction rate of the deposited metal with water to form hydroxide at room temperature. In cases when the formation of hydroxide shell does not occur, the deposited metal, such as Fe and Cu, would form the oxide shell upon exposure to air (after the working electrode is removed from the electrolyte).

For the Co film obtained with a longer deposition time of 10 s (Figure 1d), the behavior of the Co 2p spectra as a function of total sputtering time (see Figure S3 in the Supporting Information) is similar to that for the Co nanoparticles obtained by electrodeposition for 1 s (Figure 2). Evidently, the $Co(OH)_2$ shell (with Co $2p_{3/2}$ feature at 781.2 eV) is removed upon sputtering for 600 s, revealing the metallic Co core (with the characteristic Co $2p_{3/2}$ feature at 778.1 eV). Further sputtering shows the Co $2p_{3/2}$ feature at 778.7 eV for cobalt

disilicide at the interface between the Co film and Si substrate. The present XPS depth-profiling data therefore confirm that the Co nanostructured film also consists of a Co core and a $Co(OH)_2$ shell.

GIXRD patterns of Co nanoparticles and nanostructured film obtained by 1 s and 10 s electrodeposition, respectively, are shown in Figure 3. The strong sharp peak and the broad band

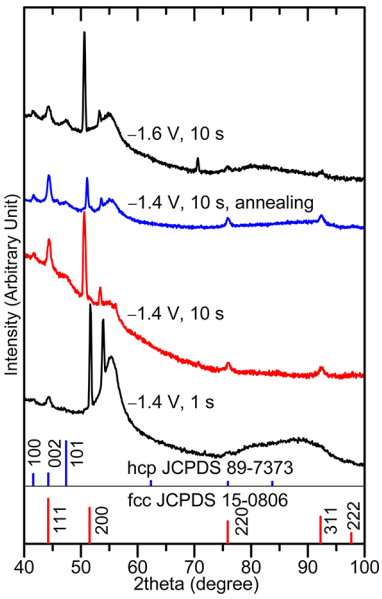

Figure 3. GIXRD patterns (in log scale) of Co nanocrystallites electrodeposited on a H−Si(100) substrate in a solution of 0.005 M $CoSO_4$, 0.2 M KCl and 0.2 M H_3BO_3 at −1.4 V (vs Ag/AgCl) for 1 s and 10 s (without and with annealing at 400 °C), and at −1.6 V (vs Ag/AgCl) for 10 s, and reference bar charts for hcp phase (JCPDS 89-7373) and fcc phase (JCPDS 15-0806) of Co powders.

in the 50-60° region could be attributed to Si(311) of the substrate.[41] Evidently, diffraction features corresponding to a mixture of hexagonal close packed (hcp) and face centered cubic (fcc) phases of metallic Co are observed. In particular, the feature at 41.6° and 47.4° are in good accord with the hcp (100) and (101) orientations, despite the hcp (100) feature being more intense than the hcp (101) feature that is contrary to the powder reference pattern (JCPDS 89-7373). The peak at 92.2° can be assigned to the fcc (311) orientation of metallic Co (JCPDS 15-0806). The peaks at 44.2° and 75.9° may have contributions from both hcp (002) and fcc (111) and from both hcp (110) and fcc (220), respectively. The ratio of the peak intensity at 41.6° [corresponding to hcp (100)] to that at 92.2° [corresponding to fcc (311)] can therefore be used to infer the relative composition of the hcp to fcc phase. The relative composition of different phases coexisting in the same sample can be estimated by comparing their relative peak intensity ratios.[42] For Co NPs obtained by the 1s-electrodeposition at −1.4 V, the composition ratio of the hcp to fcc phase cannot be deduced because the broad SiO_x feature between 75 and 95° overwhelms the feature at 92.2°. For nanostructured Co film obtained by the 10 s deposition at −1.4 V, the composition ratio of the hcp to fcc phase is found to be 0.57. Because the transition temperature from fcc to hcp has been reported to be 380 ±12 °C,[43] we set the annealing temperature to 400 °C. However, after post-annealing the nanocrystallites obtained by the 10 s deposition at 400 °C in a N_2 atmosphere for 1 h, the ratio remains unchanged (from 0.57). The absence of phase conversion could be due to size effect of the Co nanocrystallites. It has been reported that fcc Co becomes more stable when the particle size is reduced because of the lower surface energy of fcc Co than hcp Co.[44] For the nanostructured Co film obtained by a 10-s deposition at a higher deposition potential of −1.6 V, the ratio for the electrodeposits is found to be discernibly larger (2.58). This shows that the relative phase composition of hcp and fcc in the Co nanocrystallites can be controlled by simply changing the deposition potential. Control of different amounts of hcp and fcc phases in these nanocrystallites is of special interest to manipulating their magnetic properties and catalytic activities. In particular, since the magnetic anisotropy of Co changes from the *c*-axis for hcp to in-plane for fcc,[45] the coercivity of Co can therefore be changed with the application of an external magnetic field during electrodeposition. Furthermore, it has also been shown that the fcc phase has a lower catalytic activity compared to the hcp phase for such reactions as glycerol hydrogenolysis,[46] ethanol steam reforming,[47] and Fischer-Tropsch synthesis.[48] It is important to note that no diffraction feature attributable to the $Co(OH)_2$ shell is observed in all of the samples studied here, which indicates that the $Co(OH)_2$ shell is amorphous.

To demonstrate the catalytic activity of these Co NPs, we perform cyclic voltammetric scans of our Co NPs obtained by 1s electrodeposition in a solution containing 0.1 M NaOH and various concentrations of ascorbic acid (0, 2.5, 5, 10, and 20 mM). Figure 4a shows that an extremely weak oxidation peak at

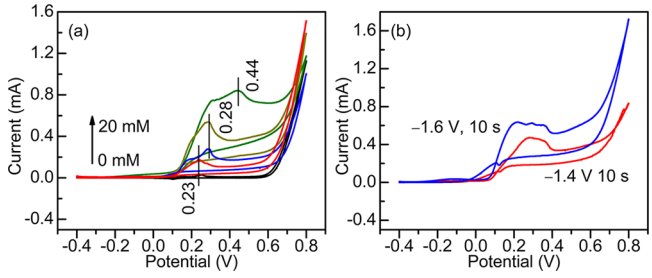

Figure 4. Cyclic voltammetric scans of (a) Co nanoparticles (obtained by 1 s electrodeposition on a H−Si(100) substrate in a solution of 0.005 M $CoSO_4$, 0.2 M KCl and 0.2 M H_3BO_3 at −1.4 V (vs Ag/AgCl)) in a solution of 0.1 M NaOH without ascorbic acid and with 2.5, 5, 10, and 20 mM of ascorbic acid; (b) Co film [obtained by 10 s electrodeposition on a H−Si(100) substrate in a solution of 0.005 M $CoSO_4$, 0.2 M KCl and 0.2 M H_3BO_3 at −1.4 V and at −1.6 V (vs Ag/AgCl)] in a solution of 0.1 M NaOH and 10 mM ascorbic acid.

0.23 V for the solution containing 0.1 M NaOH in the absence of ascorbic acid, which is attributable to the oxidation of Co^{2+} to Co^{3+} [via the reaction: $3Co(OH)_2 + 2OH^- - 2e^- \rightarrow Co_3O_4 + 4H_2O$].[20] However, for the solution containing 2.5 mM ascorbic acid, we observe an oxidation peak at 0.23 eV with a much higher current, which is clearly due to the oxidation of ascorbic acid. Upon oxidation of Co^{2+} to Co^{3+}, Co^{3+} is reduced back to Co^{2+} by a simultaneous oxidation reaction of ascorbic acid ($C_6H_8O_6$) to dehydrogenated ascorbic acid ($C_6H_6O_6$) (i.e., $2Co^{3+} + C_6H_8O_6 \rightarrow 2Co^{2+} + C_6H_6O_6 + 2H^+$).[20] By increasing the ascorbic acid concentration to 5 and 10 mM, the oxidation peak of ascorbic acid shifts to 0.28 V but with increasingly higher current. For the solution containing 20 mM ascorbic acid, the peak is found to emerge at 0.44 V. Increasing the

dx.doi.org/10.1021/am3021763 | ACS Appl. Mater. Interfaces 2013, 5, 2410−2416

concentration of ascorbic acid is expected to reduce the amount of OH^-, and because OH^- is involved in the oxidation process of $Co(OH)_2$ to Co_3O_4, the peak should shift to a higher potential. The observed current at 0.23 to 0.44 V therefore demonstrates the catalytic activity of $Co-Co(OH)_2$ core–shell NPs for the electro-oxidation of ascorbic acid. For the 0.1 M NaOH solutions with 5, 10, and 20 mM ascorbic acid, a weak oxidation peak at 0.18, 0.19, and 0.30 V, respectively, is observed (Figure 4a). The origin of this extra feature could be due to oxidation of metallic Co to Co^{3+}, followed by reduction of Co^{3+} back to Co^{2+} by a simultaneous oxidation reaction of ascorbic acid to dehydrogenated ascorbic acid.

For the Co nanostructured films obtained with 10-s deposition at −1.4 V and −1.6 V, the respective ratios of the hcp (100) to fcc (311) are 0.57 and 2.58. Assuming all the charges have been used for depositing metallic Co onto the Si substrates, the normalized electro-oxidation current of ascorbic acid in a solution of 10 mM ascorbic acid and 0.1 M NaOH for the sample electrodeposited at −1.4 V is found to be similar to that for the sample electrodeposited at −1.6 V (Figure 4b). This clearly shows that the phase composition of the Co core has no observable effect on the electro-oxidation of ascorbic acid. As the $Co(OH)_2$ shell provides the active catalytic medium for the electro-oxidation to occur, the changes in the fcc to hcp components in the Co core obtained under different deposition conditions is therefore not expected to affect this surface reaction. For the Co film electrodeposited at −1.6 V for 10 s (Figure 4b), the three weak features in the broad band region from 0.2 V to 0.4 V could be related to the changes of the surface of the Co film caused by hydrogen evolution due to a high applied electrodeposition potential.

To increase the active surface area of the working electrode, we repeat our experiment of electro-oxidation on a SiNW substrate. SEM confirms that the Si NWs provide a dramatic increase in the surface area available for the Co electrodeposition (Figure 5a), which evidently produces a continuous and uniform Co nanocrystalline film with ridgelike structures and greatly increased surface area (Figure 5b and Figure S4a in the Supporting Information). The corresponding EDX spectrum (see Figure S4a in the Supporting Information) confirms the presence of Co, whereas the Co $2p_{3/2}$ ($2p_{1/2}$) feature at 781.2 eV (797.1 eV) in the corresponding XPS spectrum (see Figure S4b in the Supporting Information) can be assigned to $Co(OH)_2$. Furthermore, its GIXRD pattern (see Figure S4c in the Supporting Information) exhibits a mixture of hcp and fcc phases of metallic Co. These data therefore support that the nanostructured Co film consists of a Co core and a $Co(OH)_2$ shell. The cyclic voltammograms of this high-surface-area, nanostructured Co coated SiNW electrode in 0.1 M NaOH solution with various concentrations of ascorbic acid are shown in Figure 5c. The response current obtained at 0.24 V is found to increase with increasing concentration of ascorbic acid. The response current does not exhibit a linear relationship in the larger concentration range from 0.1 to 100 μM. However, the current follows a linear relationship with the concentration in the concentration range below 1 μM (Figure 5d). This indicates that the nanostructured Co coated SiNW electrode can be used as a very sensitive biosensor for ascorbic acid. Indeed, a detection limit of 0.1 μM is obtained, outperforming the previously reported Co-based electrode.[20] In separate experiments, we perform cyclic voltammetric measurements in a solution of 0.1 M NaOH and 100 μM ascorbic acid for ten individual Co coated SiNW electrodes and

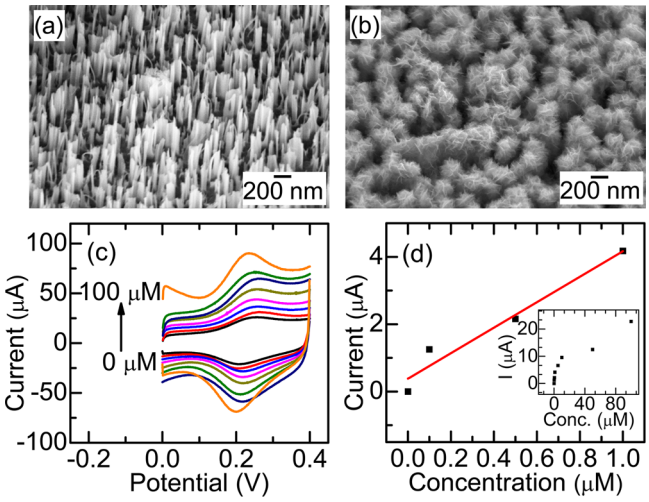

Figure 5. SEM images of (a) SiNW substrate and (b) nanostructured cobalt film electrodeposited on SiNW substrate measured at a tilting angle of 45°; (c) cyclic voltammetric scans of Co nanostructured film [obtained by 10 min electrodeposition on a SiNW substrate in a solution of 0.005 M $CoSO_4$, 0.2 M KCl and 0.2 M H_3BO_3 at −1.4 V (vs Ag/AgCl)] in a solution of 0.1 M NaOH without ascorbic acid and with 0.1, 0.5, 1, 5, 10, 50, and 100 μM of ascorbic acid; (d) variation of the response current with ascorbic acid concentration. The inset covers the wider concentration range (up to 100 μM).

obtain a relative standard deviation of 4.2% for the response current at 0.24 V. Furthermore, the response current at 0.24 V has only dropped by 5% after 20 cyclic voltammetric cycles for the same Co coated SiNW electrode. These experiments therefore indicate the excellent reproducibility and repeatability of the Co coated SiNW electrodes. We also investigate the stability of the Co-coated SiNW electrode. After storing at room temperature for over 3 months, the Co-coated SiNW electrode exhibits only a 15% reduction in the response current performed in the same experiment conditions, which illustrates its long-term stability. Finally, to demonstrate the selectivity of the Co coated SiNW electrode, we measure and compare its response current in a solution of 0.1 M NaOH and 100 μM ascorbic acid with and without 10 mM glucose and 10 mM citric acid. The essentially identical response currents so obtained indicate that the Co-coated SiNW electrode is selective to ascorbic acid in the presence of interference chemicals such as glucose and citric acid.

We also compare the sensing performance of nanostructured Co films obtained by electrodeposition for 10 min on a SiNW and a Si substrates [in a solution of 0.005 M $CoSO_4$, 0.2 M KCl and 0.2 M H_3BO_3 at −1.4 V (vs Ag/AgCl)]. Figure S5 in the Supporting Information shows their respective cyclic voltammetric scans performed in a solution of 0.1 M NaOH and 100 μM ascorbic acid. Evidently, the response current for the Co-coated SiNW electrode toward electro-oxidation of ascorbic acid is 5 times higher than that for the Co-coated bare Si substrate. The Co-coated SiNW electrode is therefore a more efficient biosensor than the corresponding Co coated Si electrode.

4. SUMMARY

In the present work, we report the formation of homogeneous metallic Co NPs on a H–Si(100) substrate by electrochemical deposition. Metallic Co NPs with a diameter of 6 nm can be easily obtained, and the particle size can be easily controlled by

the electrodeposition parameters. In accord with our depth-profiling XPS data, the Co NPs are found to consist of a Co core, with a sizable $Co(OH)_2$ shell (of about 25% in amount). Glancing-incidence XRD results further show that the metallic Co core contains both hcp and fcc phases. While such a high Co metallic core composition may have important consequence on the magnetic properties of these NPs, it is the $Co(OH)_2$ shell that provides powerful application in catalysts. We demonstrate the latter for electro-oxidation of ascorbic acid in an alkaline solution. Nanostructured Co-coated SiNW electrode with high surface area can therefore provide an important platform for potential application in biosensing.

■ ASSOCIATED CONTENT

Supporting Information

Co 2p XPS spectrum collected with a higher pass energy of 40 eV for Co NPs obtained in a solution of 0.005 M $CoSO_4$, 0.2 M KCl and 0.2 M H_3BO_3 at −1.4 V (vs Ag/AgCl) for 1 ms. Co 2p XPS depth profiling spectra for Co nanoparticles electrodeposited for 1 s and annealed at 400 °C in N_2 atmosphere for 1 h. Co 2p XPS depth profiling spectra for Co film electrodeposited for 10 s. The EDX spectrum, a magnified SEM image, Co 2p XPS spectrum and GIXRD pattern of a nanostructured cobalt film on a SiNW substrate. Cyclic voltammetric scans of Co nanostructured film on a SiNW or Si substrate in a solution of 0.1 M NaOH and 100 μM ascorbic acid. This material is available free of charge via the Internet at http://pubs.acs.org/.

■ AUTHOR INFORMATION

Corresponding Author

*Corresponding author. E-mail: tong@uwaterloo.ca.

Notes

The authors declare no competing financial interest.

■ ACKNOWLEDGMENTS

This work was supported by the Natural Sciences and Engineering Research Council of Canada.

■ REFERENCES

(1) Okiei, W.; Ogunlesi, M.; Azeez, L.; Obakachi, V.; Osunsanmi, M.; Nkenchor, G. *Int. J. Electrochem. Sci.* **2009**, *4*, 276−287.
(2) Andrews, B. S. A.; Nagendra Kumar, A. V. D. *Res. J. Pharm., Biol. Chem. Sci.* **2011**, *2*, 937−946.
(3) Burini, G. *J. Chromatogr. A* **2007**, *1154*, 97−102.
(4) Odriozola-Serrano, I.; Hernández-Jover, T.; Martín-Belloso, O. *Food Chem.* **2007**, *105*, 1151−1158.
(5) Pérez-Ruiz, T.; Martínez-Lozano, C.; Tomás, V.; Fenol, J. *Analyst* **2001**, *126*, 1436−1439.
(6) Pérez-Ruiz, T.; Martínez-Lozano, C.; Sanz, A.; Guillén, A. *J. Pharm. Biomed. Anal.* **2004**, *34*, 551−557.
(7) Spickenreither, M.; Braun, S.; Bernhardt, G.; Dove, S.; Buschauer, A. *Bioorg. Med. Chem. Lett.* **2006**, *16*, 5313−5316.
(8) Amini, M. K.; Shahrokhian, S.; Tangestaninejad, S.; Mirkhani, V. *Anal. Biochem.* **2001**, *290*, 277−282.
(9) Sheng, Q.; Yu, H.; Zheng, J. *J. Electroanal. Chem.* **2007**, *606*, 39−46.
(10) Brainina, Kh. Z.; Varzakova, D. P.; Gerasimova, E. L. *J. Anal. Chem.* **2012**, *67*, 364−369.
(11) Yue, Y.; Hu, G. Z.; Zheng, M. B.; Guo, Y.; Cao, J. M.; Shao, S. J. *Carbon* **2012**, *50*, 107−114.
(12) Hu, G. Z.; Guo, Y.; Xue, Q. M.; Shao, S. J. *Electrochim. Acta* **2010**, *55*, 2799−2804.
(13) El-Said, W. A.; Lee, J. H.; Oh, B. K.; Choi, J. W. *Electrochem. Commun.* **2010**, *12*, 1756−1759.
(14) Weng, Y. C.; Lee, Y. G.; Hsiao, Y. L.; Lin, C. Y. *Electrochim. Acta* **2011**, *56*, 9937−9945.
(15) Rohani, T.; Taher, M. A. *Talanta* **2009**, *78*, 743−747.
(16) Ferreira, R. Q.; Avaca, L. A. *Electroanal.* **2008**, *20*, 1323−1329.
(17) Zhang, Z. J.; Li, X.; Wang, C. G.; Zhang, C. C.; Liu, P.; Fang, T. T.; Xiong, Y.; Xu, W. J. *Dalton Trans.* **2012**, *41*, 1252−1258.
(18) Ensafi, A. A.; Taei, M.; Khayamian, T. *J. Electroanal. Chem.* **2009**, *633*, 212−220.
(19) Suresh, R.; Prabu, R.; Vijayaraj, A.; Giribabu, K.; Stephen, A.; Narayanan, V. *Mater. Chem. Phys.* **2012**, *134*, 590−596.
(20) Tian, L.; Bian, J. Y.; Wang, B. B.; Qi, Y. J. *Electrochim. Acta* **2010**, *55*, 3083−3088.
(21) Libertino, S.; Aiello, V.; Scandurra, A.; Renis, M.; Sinatra, F.; Lombardo, S. *Sensors* **2009**, *9*, 3469−3490.
(22) Kwon, J. H.; Saly, M.; Halls, M. D.; Kanjolia, R. K.; Chabal, Y. J. *Chem. Mater.* **2012**, *24*, 1025−1030.
(23) Pető, G.; Molnár, G.; Bogdányi, G.; Guczi, L. *Catal. Lett.* **1994**, *26*, 383−392.
(24) Guczi, L.; Pető, G.; Beck, A.; Pászti, Z. *Topics Catal.* **2004**, *29*, 129−138.
(25) Koch, S. A.; Palasantzas, G.; Vystavel, T.; De Hosson, J.; Th, M.; Binns, C.; Louch, S. *Phys. Rev. B* **2005**, *71*, 085410−5.
(26) Kalska, B.; Paggel, J. J.; Fumagalli, P.; Hilgendorff, M.; Giersig, M. *J. Appl. Phys.* **2002**, *92*, 7481−7485.
(27) Leo, G.; Chushkin, Y.; Luby, S.; Majkova, E.; Kostic, I.; Ulmeanu, M.; Luches, A.; Giersig, M.; Hilgendorff, M. *Mater. Sci. Eng. C* **2003**, *23*, 949−952.
(28) Chushkin, Y.; Ulmeanu, M.; Luby, S.; Majkova, E.; Kostic, I.; Klang, P.; Holý, V.; Bochníček, Z.; Giersig, M.; Hilgendorff, M.; Metzger, T. H. *J. Appl. Phys.* **2003**, *94*, 7743−7748.
(29) Curry, M. L.; Crews, K.; Warke, V.; Bakker, M. G.; Hong, K. L.; Mays, J.; Britt, P.; Li, X. F.; Wang, J. *J. Vac. Sci. Technol. A* **2011**, *29*, 031401−5.
(30) Moina, C. A.; de Oliveira-Versic, L.; Vazdar, M. *Mater. Lett.* **2004**, *58*, 3518−3522.
(31) Kern, W. In *Handbook of Semiconductor Wafer Cleaning Technology*; Kern, W., Ed.; Noyes: Park Ridge, NJ, 1993.
(32) Shi, J.; Hara, Y. H.; Sun, C. L.; Anderson, M. A.; Wang, X. D. *Nano Lett.* **2011**, *11*, 3413−3419.
(33) Santos, J. S.; Matos, R.; Trivinho-Strixino, F.; Pereira, E. C. *Electrochim. Acta* **2007**, *53*, 644−649.
(34) Zsoldos, Z.; Hoffer, T.; Guczi, L. *J. Phys. Chem.* **1991**, *95*, 798−801.
(35) Kim, M. H.; Choo, K. H. *Catal. Commun.* **2007**, *8*, 462−466.
(36) Seah, M. P. Quantification of AES and XPS. In *Practical Surface Analysis by Auger and X-ray Photoelectron Spectroscopy*; Briggs, D., Seah, M. P., Eds.; Wiley, New York, 1983; p 204.
(37) Chang, J. J.; Liu, C. P.; Hsieh, T. E.; Wang, Y. L. *Surf. Coatings Technol.* **2006**, *200*, 3314−3318.
(38) Zhao, L. Y.; Heinig, N.; Leung, K. T. *J. Phys. Chem. C* **2012**, *116*, 12322−12329.
(39) Zhao, L. Y.; Jalili, H.; Panjwani, N.; Chan, T.; He, Z. H.; Heinig, N. F.; Leung, K. T. *Electrochem. Solid -State Lett.* **2007**, *10*, K47−49.
(40) Radi, A.; Pradhan, D.; Sohn, Y. K.; Leung, K. T. *ACS Nano* **2010**, *4*, 1553−1560.
(41) Cho, B. O.; Chang, J. P.; Min, J. H.; Moon, S. H.; Kim, Y. W.; Levin, I. *J. Appl. Phys.* **2003**, *93*, 745−749.
(42) Chung, F. H.; Smith, D. K. In *Industrial Applications of X-Ray Diffraction*; Chung, F. H., Smith, D. K., Ed.; Marcel Dekker: New York, 2000.
(43) Giber, J.; Drube, R.; Dose, V. *Appl. Phys. A* **1991**, *52*, 167−170.
(44) Ram, S. *Mater. Sci. Eng. A* **2001**, *304*−*306*, 923−927.
(45) Vaz, C. A. F.; Bland, J. A. C.; Lauhoff, G. *Rep. Prog. Phys.* **2008**, *71*, 056501−78.
(46) Cao, Y. B.; Zhang, X.; Fan, J. M.; Hu, P.; Bai, L. Y.; Zhang, H. B.; Yuan, F. L.; Chen, Y. F. *Cryst. Growth Des.* **2011**, *11*, 472−479.

(47) Lin, S. S. Y.; Kim, D. H.; Ha, S. Y. *Appl. Catal. A* **2009**, *355*, 69−77.
(48) de la Peña O'Shea, V. A.; de la Piscina, P. R.; Homs, N.; Aromí, G.; Fierro, J. L. G. *Chem. Mater.* **2009**, *21*, 5637−5643.